2019-04-01

Modeling Piezoresistive Effects in Flexible Sensors

Marianne E. Clayton
Brigham Young University

Modeling Piezoresistive Effects in Flexible Sensors

Marianne E. Fletcher Clayton

A thesis submitted to the faculty of
Brigham Young University
in partial fulfillment of the requirements for the degree of

Master of Science

David T. Fullwood, Chair
Anton Bowden
Andy George

Department of Mechanical Engineering

Brigham Young University

ABSTRACT

Modeling Piezoresistive Effects in Flexible Sensors

Marianne E. Fletcher Clayton
Department of Mechanical Engineering, BYU
Master of Science

This work describes a model of the piezoresistive behavior in nanocomposite sensors. These sensors are also called flexible sensors because the polymer matrix allows for large deformations without failure. The sensors have conductive nanoparticles dispersed through an insulative polymer matrix. The insulative polymer gaps between nanoparticles are assumed to be possible locations for electron tunneling. When the distance between two nanoparticles is small enough, electrons can tunnel from one nanoparticle to the next and ultimately through the entire sensor. The evolution of this gap distance with strain is important to understand the overall conductivity of the strain sensor. The gap evolution was modeled in two ways: (1) applying Poisson's contraction to the sensor as a homogenous material, referred to as Simple Poisson's Contraction (SPC) and (2) modeling the nanoparticle-polymer system with Finite Element Analysis (FEA). These two gap evolution models were tested in a random resistor network model where each polymer gap was treated as a single resistor in the network. The overall resistance was calculated by solving the resistor network system. The SPC approach, although much simpler, was sufficient for cases where various orientations of nanoparticles were used in the same sensor. The SPC model differed significantly from the FEA, however, in cases where nanoparticles had specific alignment, e.g. all nanoparticles parallel to the tensile axis. It was also found that the distribution used to determine initial gap sizes for the polymer gaps as well as the mean of that distribution significantly impacted the overall resistivity of the sensor.

Another key part of this work was to determine if the piezoresistivity in the sensors follows a percolation type behavior under strain. The conductance versus strain curve showed the characteristic s-curve behavior of a percolative system. The conductance-strain curve was also compared to the effective medium and generalized effective medium equations and the latter (which includes percolation theory) fit the random resistor network much more closely. Percolation theory is, therefore, an accurate way to describe this polymer-nanoparticle piezoresistive system.

Finally, the FEA and SPC models were compared against experimental data to verify their accuracy. There are also two design problems addressed: one to find the sensor with the largest gauge factor and another to determine how to remove the characteristic initial spike in resistivity seen in nanocomposite sensors.

Keywords: nanocomposite sensor, percolation theory, piezoresistivity, quantum tunneling

ACKNOWLEDGEMENTS

I would like to thank Dr. Fullwood for his support and mentorship through this project and for pushing me farther than I thought I could go. I would also like to thank Dr. Bowden and Dr. George for their ideas and willingness to be on my committee. I recognize the contributions of previous students including Adam Bilodeau for his work in Finite Element Analysis and David Wood for his nanoindentation testing. I'm grateful to my family and friends who supported me and encouraged me. I am also endlessly grateful to my husband, Sam, who spent countless hours listening to me problem-solve and looking through broken code, without whom I would not have been able to complete this project.

Funding for this research was provided by the National Science Foundation under grant numbers CMMI-1538447. Any opinions, findings, and conclusions or recommendations expressed in this material are those of the author and do not necessarily reflect the views of the National Science Foundation.

TABLE OF CONTENTS

LIST OF TABLES

LIST OF FIGURES

1 INTRODUCTION

1.1 Conductive Polymer Composites

Insulative polymers can be made into conductive polymer composites by the addition of some kind of conductive filler. The combination of polymer and conductive filler is referred to as a conductive polymer composite. There are several applications for conductive polymer composites including electromagnetic interference shielding [1-3], neural electrodes [4], films for fuel cells [3, 5-7], and sensors [8-10]. The research presented here will focus on the use of conductive polymer composites made with nanoparticles as sensors in biomechanical applications. Biomechanical applications for flexible sensors include measuring range of motion for joints [11], pulse [12], and breathing [13]. These sensors must be flexible enough to not restrict motion as well as sensitive to small changes in strain.

In order to achieve the desired flexibility, the majority of nanocomposite sensors use rubber-like polymers as the matrix (e.g. PDMS [14, 15], natural rubbers [13, 16]). There are many different conductive fillers including carbon black [14, 15, 17, 18], carbon nanotubes [17-19], or metal nanowires [12, 20]. The sensors in this study were made of silicone rubber (Ecoflex or Sylgard 184) with nickel nanoparticles from Conductive Composites in Heber, UT.

Since the matrix polymer is fundamentally an insulator, electrical conductivity across such materials depends upon the presence of connected networks of the conductive filler. Various studies have investigated the relationship between volume fraction of filler, and resultant

material conductivity [21-26]. As the percentage of filler increases, a threshold is crossed, after which the probability of a connected pathway of filler spanning the entire sample is equal to one. At this point, the conductivity increases rapidly as more filler is added. However, for the sensor applications, the volume fraction of filler is not changing; instead, we are interested in understanding and predicting sensor piezoresistivity – i.e. the relationship between applied strain and sensor conductivity, for a constant volume fraction of filler. In the literature, there are several theories for piezoresistive response for this type of material. These include bulk sample volume change, filler particle realignment, and the changes in tiny gaps between neighboring particles facilitating (or blocking) electron flow along conductive pathways [27-29]. Only the third option mentioned can explain the massive changes in conductivity witnessed for this type of material, with the conductivity across a given gap being controlled by quantum tunneling (as explained below). However, no in-depth study of the evolution of the distribution of gaps between particles, and resultant impact on sensor conductivity, has been undertaken.

This paper seeks to contribute to the current state of the art in two ways: (1) To undertake a detailed analysis of gap evolution in a high-aspect ratio nanoparticle conductive polymer composite, and the resultant relationship between sensor strain and conductance; and (2) To determine whether the resultant piezoresistive phenomenon should be modeled in terms of percolative behavior, or using standard effective medium type approaches. The structural evolution of potential composites is modeled using a finite element approach, focused on gap geometry between ideal cylindrical neighboring nanoparticles. The overall sensor conductivity is determined using a random resistor network, for an assumed regular arrangement of such nano-gaps. And the resultant conductivity values are compared with predictions from percolation and effective medium theories.

1.2 Sensor Modeling

The nanocomposite sensors experience a phenomenon called piezoresistivity because of the combination of the insulative polymer and conductive nanoparticles. If the network were perfectly electrically connected, the overall material conductivity would simply relate to the volume fraction of filler; however, the conductivity is much lower than such a model would predict, and hence is dominated by the resistance between neighboring filler particles in the network. When the polymer gap between neighboring conductive particles is small enough, electrons can move from one nanoparticle to the next through the entire sensor. As the sensor experiences strain, the nanoparticles move in relation to each other which changes the distribution of gaps between neighbors, and the overall electrical response of the sensor.

As briefly mentioned above, current research seeks to be able to predict the electrical behavior of the sensor (resistance) based on strain. Because the piezoresistive effects are dominated by the size of the polymer gap between neighboring conductive particles, modeling how those gaps change with strain is a key component of any predictive model. A simplified analysis of gap evolution with strain was previously reported by Johnson et al. [30]. This research will analyze and compare a much more detailed geometrical model of gaps between particles with the Johnson model. The previous model is computationally simpler and assumes that the material can be modeled as an isotropic and homogenous system; furthermore, the gap distribution is assumed to change using a simple Poisson's contraction model based upon the direction of the shortest vector across a gap between particles. The current approach will be based upon Finite Element Analysis (FEA) data, where the nanoparticles are modeled as pairs of cylinders with the full geometrical details of their local structural arrangement taken into account. More details about these models are given below.

1.2.1 Quantum Tunneling

As mentioned, the nano-composite sensors examined in this thesis experience large drops in resistance when the material is strained, indicating a mechanism that is highly sensitive to the evolving gap between neighboring particles; the only theory of electrical resistance between neighboring nanoparticles that is consistent with observed behavior is that of quantum mechanical tunneling. Quantum tunneling is described by quantum mechanics and explains how an electron can cross a potential energy barrier that would block electrical flow by classical theories. Each gap between two nanoparticles can be considered as a potential location for quantum tunneling [19, 30-36]. Equation 1 shows the tunneling resistivity across a gap between two nanoparticles, where ρ is tunneling resistivity, h is Planck's constant, e is the charge of an electron, m_e is the mass of an electron, λ is barrier height, and s is the junction gap distance [37].

$$\rho(s) = \frac{h^2}{e^2\sqrt{2m_e\lambda}} \exp\left(\frac{4\pi\sqrt{2m_e\lambda}}{h} s\right) \quad 1$$

Barrier height (λ) is the electrical potential difference between the two nanoparticles and junction gap distance (s) is the distance between the two nanoparticles. Both of these parameters were experimentally measured for polymer matrices using the procedure described by Koecher [38]. In order to determine barrier height, a conductive nano-indenter was slowly pushed through a thin layer of polymer on a nickel chip, and the gap plotted against resultant conductivity between the probe and plate; the barrier height was thus inferred. We note that this was for a nickel plate and a conductive diamond tip; we assume that the barrier height between to nickel contacts will be similar. Table 1-1 shows the values for junction gap distance used in this work from data collected in May 2017.

Table 1-1. Experimental values for barrier height of the polymers in this work. The barrier height was measured using the nano-indentation method described in Koecher [38].

Polymer	*Barrier Height (eV)*
Sylgard 184	0.47
Ecoflex	0.27

The average gap junction distance (s) was determined with dielectric spectroscopy and the Cole-Cole equation as explained in Koecher [38]. The junction was modeled as a resistor and a capacitor in parallel. The junction gap distance can then be calculated from the characteristic frequency.

In this work, the nanoparticles are assumed to be cylindrically shaped for the FEA model. As can be seen in Figure 1-1 of the as-manufactured nanostrands, the particles actually have a very branched structure. However, before being used in the conductive composite sensors this network is broken into small particles, and subsequently pushed through a screen to break the network into even smaller nanoparticles. The branched nature of the nanoparticles may impact the initial range of orientations of the nanoparticles, and would certainly affect attempts at physically aligning the nanoparticles in manufacturing; but where the branches cross, the high aspect ratio means that they still behave as two long rods, locally. Hence, while the cylindrical assumption does not perfectly describe the overall shape of the nanoparticles, at the local level (in the vicinity of a given junction between neighbors) the approximation of cylindrical shape is expected to be sufficient.

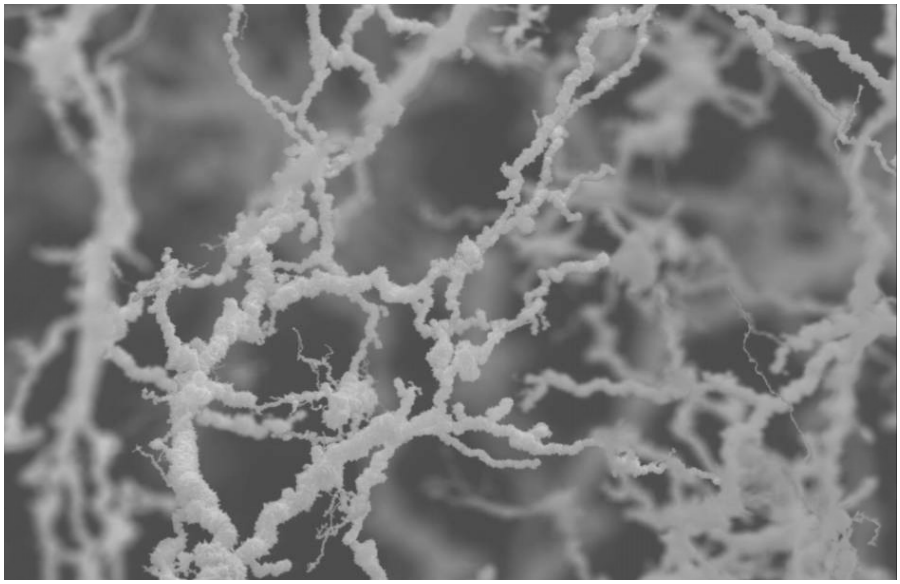

Figure 1-1. Photograph of nickel nanostrands from Conductive Composites taken at 2500x [39].

The junction gap distance (s) quantifies the distance across which an electron needs to tunnel in order for electricity to flow across the gap; it is assumed to represents that smallest gap between two particles. In order for the resistivity described by Equation 1 to be used to quantify electrical flow, the area of particle separated by this distance is required. The models used in the previous works [30] and in this work assume a constant area between particles to calculate junction gap distance. This does not account for cases such as where nanoparticles are exactly parallel and the entire length of the nanoparticles would be possible for tunneling. The experimentally-determined s from dielectric spectroscopy also assumed a constant area [38], so any error from the value of the area is compensated somewhat in the s determined by the model.

1.2.2 Percolation Theory

Conductive composites, such as those discussed here, represent a quintessential percolation-type system. The metal filler has conductivity several orders of magnitude higher

than the polymer matrix; hence overall electrical resistance through the material is dominated by the presence of connected paths of filler. The difference in resistivity between the nickel nanoparticles and the polymer gap is many orders of magnitude. The resistivity of pure nickel is on the order of $10^{-8}\ \Omega \cdot \mathrm{m}$ and the resistivity of a 1 nm gap for Ecoflex polymer (roughly the size of one polymer chain representing the smallest possible gap size) is on the order of $10^{-2}\ \Omega \cdot \mathrm{m}$. As the volume fraction of filler increases, a critical volume fraction, ϕ_c, is reached, when connected pathways begin to form and conductivity increases rapidly [40].

For the sensing material of interest to this paper, the volume fraction of filler remains constant, but the distribution of gap distances between particles evolves with strain, thus modifying the conductivity of potential pathways across the sensor. It has been hypothesized that the dramatic change in gap conductivity when the sample is strained is analogous to increasing (or decreasing) the volume fraction of conductive segments in the material, leading to a percolation-type behavior, with a critical strain at which conductivity increases rapidly [41]. One objective of this paper is to determine whether a percolation-based model reflects the actual behavior of the system.

One approach to modeling the piezoresistive behavior in conductive polymer composite sensors is with a generalized effective media equation (GEM) [41] which modifies the effective media theory to include a percolation threshold and critical coefficients. If a composite is assumed to be composed of insulating matrix, and conductive filler phases, with perfect conductivity between filler particles that touch each other (i.e. no quantum tunneling gaps), then the GEM equation is shown in Equation 2 where ϕ is the volume fraction of filler, σ_m is the conductivity of the neat polymer matrix, σ_f is the conductivity of the filler material, σ_b is the

conductivity of the bulk material, and s and t are critical exponents. A is a constant related to the percolation threshold, ϕ_c (see Equation 3).

$$\frac{(1-\phi)\left(\sigma_m^{1/s}-\sigma_b^{1/s}\right)}{\sigma_m^{1/s}+A\sigma_b^{1/s}}+\frac{\phi\left(\sigma_f^{1/t}-\sigma_b^{1/t}\right)}{\sigma_f^{1/t}+A\sigma_b^{1/t}}=0 \qquad 2$$

$$A=\frac{1-\phi_c}{\phi_c} \qquad 3$$

Many conductive polymer composite models use the GEM equation [3, 10, 42-46]. However, previous research has also highlighted the fact that the resistance across the percolating network is not defined simply by the resistance of the filler particles [47-49]. The actual resistance of the filler is orders of magnitude smaller than the resistance of the nano-scale polymer gaps between particles; i.e. the network resistance is dominated by the quantum tunneling resistance across these tiny gaps. Hence a revised model is required that somehow accounts for the distribution of gaps rather than the volume fraction of filler.

Several models combine percolation theory and quantum tunneling into one model [30, 47, 48, 50, 51]. Johnson, et al. [30] combined quantum tunneling with Equation 2 by assuming that, for a given volume fraction of filler, there is a certain distribution of gaps between filler particles that can be thought of as a lattice of switches between components of the filler network. The number fraction of tunneling junctions in this lattice is given by Q, and a critical number fraction of tunneling junctions (Q_c) is used in the percolation theory, rather than the filler volume fraction (ϕ) and critical volume fraction (ϕ_c). Equation 2 was used to calculate the resistivity of the matrix across the gap (ρ_m) as a function of barrier height.

One question that remains to be answered is whether or not the change in tunneling resistance with gap as the sample is strained, and the resultant overall network resistance, follows percolation type behavior. If the resistance change across the gaps does not follow a typical

percolation on/off behavior, then the behavior could be modeled with effective media theories instead of the GEM equation. The validity of the percolation model versus a mean field theory will be tested by simulating the entire resistance network; each gap will be modeled as a resistor and the entire network simulated as a random resistor network to find bulk resistance.

1.2.3 Evolution of Particle Geometry

Another important aspect of a piezoresistive model involves the change of the geometry between two filler particles with strain. The resistance of a particular gap has an exponential relationship with gap size according to Equation 3, so small changes in gap distance have a large impact on the overall resistance. The previous simplistic model by Johnson [30] assumed a random distribution of particle orientations that remained constant when the material was strained (i.e. the vector connecting the two closest points between a pair of neighboring particles did not change direction under strain);. Gap distances changed according to a Poisson contraction model; the gaps that aligned with the tensile direction were lengthened, while gaps in a perpendicular direction were shortened according to the Poisson's ratio. Figure 1-2 shows a visual representation of the changes in gap distance according to orientation of the vector between the two closest points, relative to the tensile axis. This model will be referred to as the Simple Poisson's Contraction model (or SPC) in this work.

The SPC model would be approximately correct if the filler particles and matrix had similar elastic modulae, and if only small strains were assumed. However, the nickel particles are stiffer than the silicone matrix by several orders of magnitude, causing severe realignment of the particles (and affiliated gaps) under large strains. Finite element analysis (FEA) is required in order to better estimate the subsequent gap evolution and resultant conductivity. In addition to having a more complete model for evolution of particle gap with strain, another important

benefit of more detailed analysis is the potential to design a sensor to behave in a desired way. For example, a study of the relationship between initial particle alignment and resultant sensor behavior could motivate a sensor design with optimized particle orientation in order to achieve a high gauge factor, or a specific characteristic resistance.

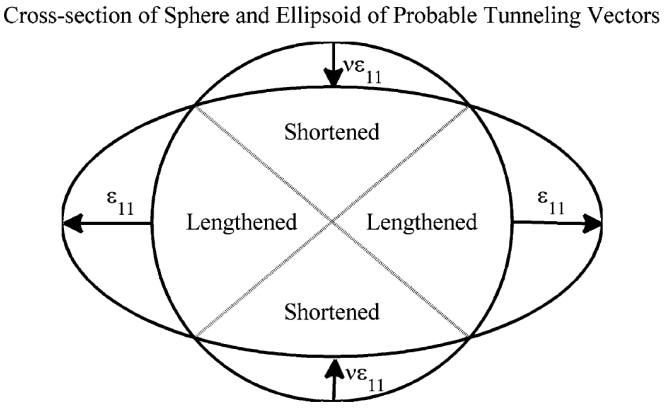

Figure 1-2. Visual representation of how the material changes according to Poisson's ratio. Figure from Johnson [30].

2 METHODS

2.1 Evolution of Particle Gap Distribution from Finite Element Analysis

2.1.1 Basic Geometry

The finite element analysis (FEA) focuses on the geometrical evolution of two neighboring nanoparticles, and the subsequent modification to the gap between them with strain. Figure 2-1 shows a two-dimensional representation of the basic geometry used in the FEA model (not to scale.) The cylindrical nanoparticles are placed within a block of pure silicone. Outside of the silicone cell is a larger block of homogenous material that combines the properties of the nickel nanoparticles and silicone matrix using the law of mixtures.

Boundary conditions were applied to the geometry of Figure 2-1 in the form of constraints to x-direction motion on one face, and application of a specified displacement in the x-direction on the opposite face as shown in Figure 2-2. The dotted line shows an example of a set displacement. There are constraints on the left side (according to Figure 2-2) in the z-direction as well, but the figure just shows two dimensions.

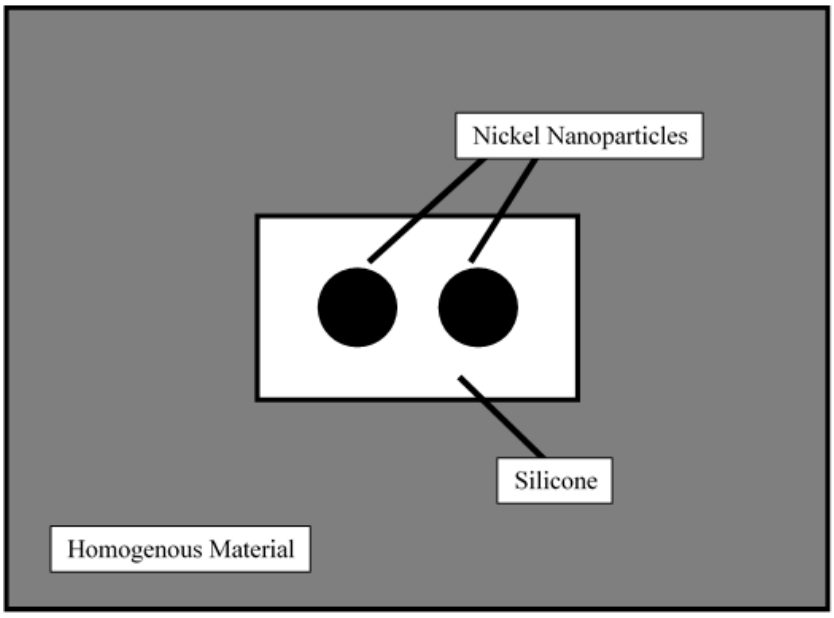

Figure 2-1. Two-dimensional representation of the basic geometry for FEA. The nanoparticles are surrounded by a small amount of silicone and then by a larger matrix of homogenous material that combines properties of silicone and nanoparticles. Note that figure is not to scale.

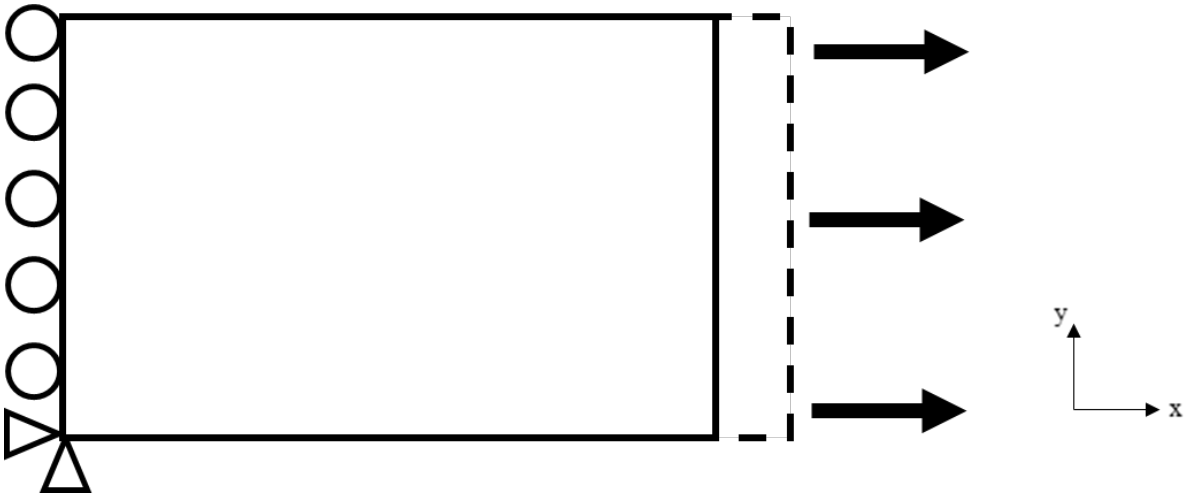

Figure 2-2. Two-dimensional diagram of the constraints in FEA geometry. The dotted line represents a set displacement.

The angle of each nanoparticle was specified with respect to the other nanoparticle and the tensile axis using four angles: θ, ϕ, α, β. Figure 2-3 shows a representation of how the axis

is affected by the angles and how they affect the positioning of the nanoparticles. In Figure 2-3 the tensile direction is along the x-axis. The angles are applied to the orientation of the system as follows: (1) align both particles with the y-axis, one vertically above the other, with the origin halfway between; (2) rotate both particles about the z-axis in the right-handed sense, by angle θ; (3) rotate the $z = z'$-axis (and the two particles) about the y'-axis by ϕ, in the right-handed sense; (4) rotate the bottom particle by α about the z''-axis, in the right-hand sense; (5) rotate the top particle by β about the z''-axis in the right-hand sense. Thus ϕ and θ affect the axis of the nanoparticles with respect to the tensile axis, and α and β rotate the nanoparticles within the coordinates defined by ϕ and θ.

Initial gap sizes of 2, 3.25, 4.5, and 5.75nm were used. In an actual sensor, the nanoparticles appear to be pushed together somehow by the manufacturing process or attraction to each other so that they polymer gaps between nanoparticles are very small. Without the nanoparticles being pushed together in some way, the gaps would be much larger. Hence, the thin layer of resin pushing back controls the distance between the particles. A layer of polymer that is one molecule thick would be approximately 1nm [30]. If both nanoparticles had an 1nm thick adsorbed layer, the total gap would be 2nm. Therefore, 2nm is assumed to be the smallest possible gap. Gaps below 2nm also have resistances close to the range of typical conductive materials (about $10^{-4}\ \Omega \cdot \mathrm{m}$) according to Equation 1 and gaps up to 5.75nm were chosen to show that even larger initial gaps with resistivities that are in the range of insulative materials (about $10^{6}\ \Omega \cdot \mathrm{m}$) can decrease to the conductive range with strain. These five distances were used as bins where any initial gap distance could be assigned and change in gap distance with strain calculated. Any gaps smaller than 2nm were assigned to the 2nm bin and any gaps larger than 5.75nm were assigned to the 5.75nm bin.

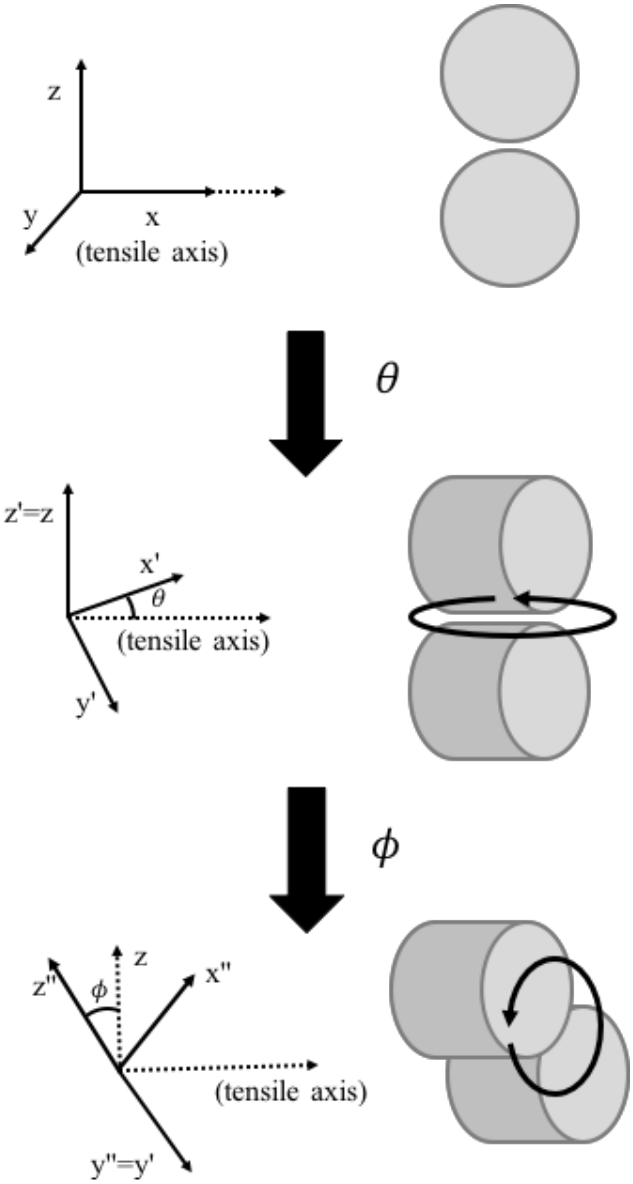

Figure 2-3. Representation of the angles used in FEA. θ and ϕ define the coordinate axes of the fibers with respect to the tensile axes as shown in the figure. The angles α and β are then the rotations of individual nanoparticles about z'' in the right-hand sense.

2.1.2 Model Details

Finite element analysis for this work was done in ANSYS 17.2. The simulated nanoparticles were each cylinders with a radius of 50 nm and 1000 nm long. As stated earlier, although the physical character of the nanoparticles is branched, their high aspect ratio means that any effects of particle curvature are generally at a distance, and the assumption of local linearity should be sufficient. The modeled dimensions were chosen to be within typical values for the radius and aspect ratios. Typical radii range from 25-250nm and aspect ratios of NiNs range from 5-50 [52]. The silicone region had a side length 1200nm and the homogenous material was a block of 3600 nm side length (see Figure 2-1). All sub-volumes used element type SOLID187. The properties used in the FEA model for each of the materials are listed in Table 2-1. The density and Poisson's ratio for the homogenous material assumed a volume fraction of 0.54% filler to simulate the behavior of the rest of the sensor.

Table 2-1. Material properties used in FEA for the three different materials in Figure 2-1.

Material	*Young's Modulus (GPa or kg/nm^2)*	*Density (kg/nm^3)*	*Poisson's Ratio (nm/nm)*
Nickel Nanoparticles	207	8.91e-12	0.31
Silicone	1.5e-3	1.29e-21	0.45
Homogenous Material	0.57	1.33e-21	0.449

The mesh for all volumes used tetrahedral elements. The mesh of the nanoparticles divided each cylinder into sections that were about 33 nm in length. The silicone block was divided into elements comprised of 8nm segments and the homogenous block was divided into

10nm segments. These element sizes were chosen after a sensitivity analysis to ensure that the FEA model converged on a consistent prediction of behavior for the system.

2.1.3 Change in Gap Distance

The information required by the random resistor model to calculate sensor resistivity is the minimum gap between neighboring nanostrands. The output of the FEA program is the position of each of the nodes at each strain interval. The gap distance between the particles is calculated by finding the smallest distance between any node on the first nanoparticle and any node on the second nanoparticle.

In order to interpolate the FEA data, the results of minimum gap vs strain were fitted to curves. The gaps that decreased with strain followed an approximately exponential decay; hence an exponential curve was fit to the data, with an assumed asymptote. The initial gap between the particles is governed by the presence of an adsorbed layer of silicone on the nickel; hence it was assumed that the minimum distance between particles was defined by the thickness of a single polymer molecule (assumed to be approximately 1nm [30, 53].) For gaps that increased with strain, the nature of the initial increase had a significant impact on the change in junction resistance; but the impact dropped of rapidly since the tunneling resistance increases exponentially with gap distance (see Equation 1). Therefore, the characteristics of the fitting curve were only significant at small gap increases; gaps that increased 3nm beyond the initial gap size had negligible conductance compared to the initial conductance . Hence, the fit used in this work was an inverse exponential function with an asymptote of 3nm greater than the initial gap distance. Figure 2-4 shows an example of the shapes of the exponential curves used to fit the FEA data. The dots represent the actual data from the FEA simulation and the lines are the exponential fits. The dotted line is FEA data from a gap with 3.25nm initial size with orientation

(0,0,0,0) for $(\theta, \phi, \alpha, \beta)$. The dotted line approaches an asymptote of 1nm. The dotted line is FEA data from a gap with initial size of 3.25nm and an orientation of (0,0,60,90) for $(\theta, \phi, \alpha, \beta)$. The dotted line approaches an asymptote of 6.25nm – 3nm bigger than the initial gap size.

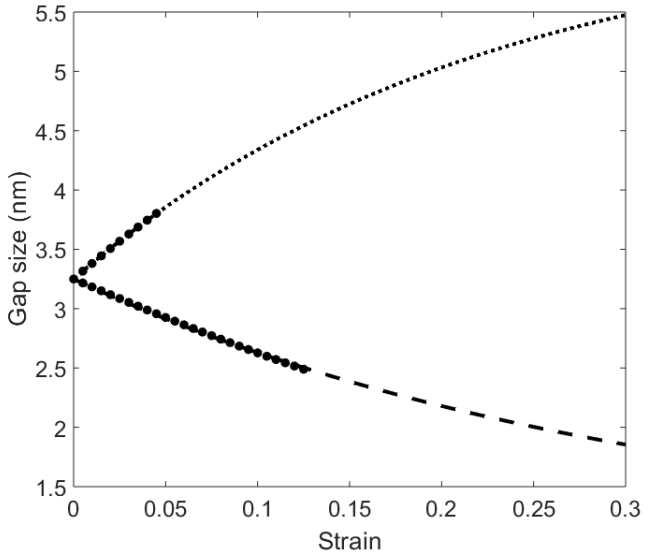

Figure 2-4. Example curve fits of FEA data for gap size versus strain. The dashed line is for a gap with an initial distance of 3.25nm and nanoparticle orientations of (0,0,0,0) for $(\theta, \phi, \alpha, \beta)$. The dotted line is a gap with an initial distance of 3.25nm and nanoparticle orientations of (0,0,60,90) for $(\theta, \phi, \alpha, \beta)$.

The curve fit of the FEA data also allowed extrapolation of gap size calculation to larger values of strain, beyond those considered by the model. The data from the FEA model covered a range of 0-25% strain. Beyond 25% strain, convergence was sometimes very slow, due to the nonlinear nature of the problem. Furthermore, the resistance model was generally not very sensitive to small errors in gap determination at higher strain values, due to the asymptotic nature of the gap evolution curves. The typical range of the sensors is between 0-30% for biomechanical applications; hence, the assumed maximum strain for most purposes in this paper is 30%, a relatively small extrapolation beyond the model calculations. The extrapolation also

seems reasonable because there are physical limits on the range of the gap even at high values of strain, i.e. the absorbed layer thickness of the polymer being the lower constraint and material flexibility being the upper constraint.

2.2 Random Resistor Network

The accuracy of the analytical model (using GEM with the SPC or FEA gap orientation model) was determined by creating a random resistor network. Each resistor represents a gap between two nanoparticles. The nodes between resistors represent the nanoparticles themselves, but because the resistance of the nickel is so small compared to the resistance of the polymer only the resistance of the gap is considered in the resistor network. Figure 2-5 shows a representation of the resistor network in two dimensions, although a three-dimensionally version was actually used. The resistors are attached to a voltage source on one side and to ground on the other.

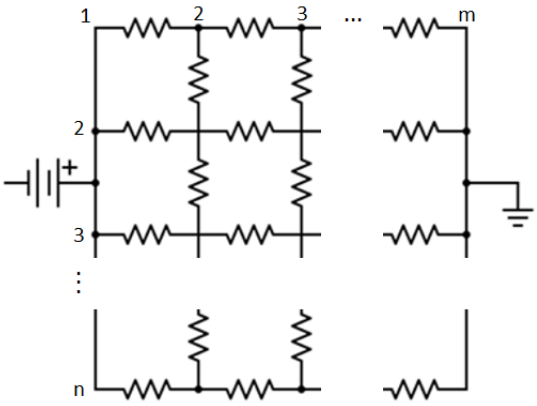

Figure 2-5. Two-dimensional example of a resistor network. The actual random resistor network model used a similar geometry but in three dimensions.

The geometry of the random resistor network in three dimensions is a cubic lattice. The junction gaps in a sensor will not have the same cubic configuration, but it is reasonable to assume that that because of the aspect ratio of the nanoparticles, each is probably connected to at least several other particles just as each node is connected to others in the lattice.

The value of the resistance between each node comes from quantum tunneling theory. The gap distance was used as the junction gap distance (s) in Equation 1 to calculate the resistivity of the gap. With increasing strain, the value of the gap distance (and hence the resistivity) changes according to FEA or SPC gap orientation models. Then the resistance (R) is calculated from resistivity (ρ) by using the gap distance for the length (s) and the surface area (A) of the tunneling junction (Equation 4).

$$R = \frac{\rho\, s}{A} \qquad 4$$

The surface area available for electron tunneling depends on how much of the nanoparticles are overlapping. If the nanoparticles are parallel, electrons can tunnel along the entire length of the nanoparticles, but at other orientations there is a much smaller available for possible tunneling. This area was calculated by approximating each nanoparticle as a rectangle using the length (1000nm) and half of the radius (25nm). The entire diameter of a cylinder would not be available surface area for electron transfer at the same time, so a value of half of the radius was used to approximate the spherical effect. The distance of half of the radius was used as a simple approximation to account for differing amounts of overlap depending on close the nanoparticles are to each other. The area was calculated for each nanoparticle orientation based on the α and β angles (see Figure 2-3). If the nanoparticles were perpendicular to each other, the area was calculated as the smallest possible area (i.e. a square with 25nm sides); if the nanoparticles were parallel to each other the area was the largest possible area (i.e. a 1000nm by

25nm rectangle). Other angles were assigned between the maximum and minimum areas using a linear relationship. Figure 2-6 shows examples of the area for electron transfer for different nanoparticle orientations. The white rectangles are the nanoparticles and the darker area is the surface area for electron tunneling.

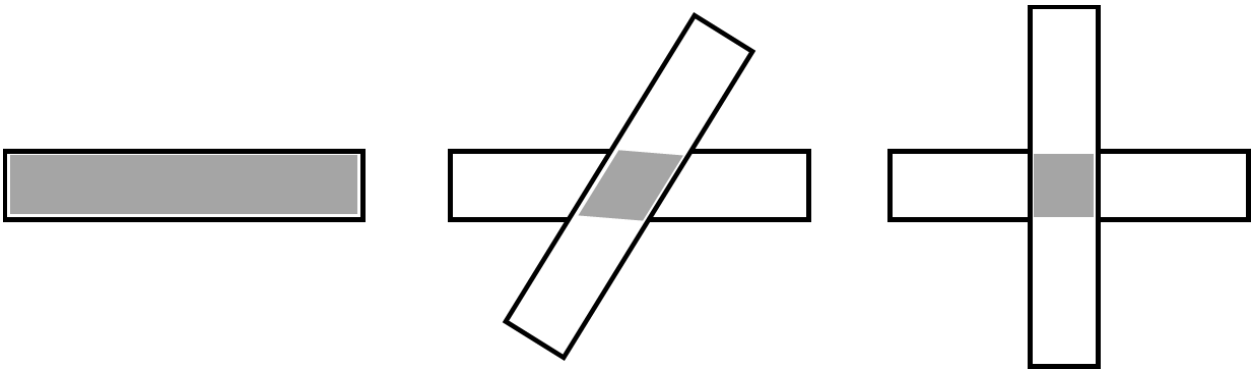

Figure 2-6. Examples of the area available for electron tunneling for different values of α and β. The white rectangles are the nanoparticles and the darker areas are where the nanoparticles overlap and could allow electrons to tunnel.

Using the calculated areas as described previously, the resistivities calculated from the tunneling equation (Equation 2) can be converted to resistances to be used in the random resistor network model. The random resistor network model calculates an overall resistance for the entire sensor as a whole. This resistance was then converted back into resistivity using the dimensions of a single nanoparticle – 1000nm in length and 50nm radius. The dimensions of the entire sensor were estimated by multiplying the dimensions of a single nanoparticle by the number of nanoparticles in the network. It was assumed that approximately half of the nanoparticles were aligned with the tensile axis and about half perpendicular to the tensile axis. Converting resistance into resistivity ultimately allowed for a better comparison with experimental data explained later in this work.

3 RESULTS AND DISCUSSION

3.1 Comparison of Gap Orientation Models (FEA and SPC)

3.1.1 Orientation

The first thing to be analyzed in this paper is the accuracy of the prediction of gap evolution with strain using the Simple Poisson's Contraction model (SPC) compared with the more detailed FEA approach. Various geometrical distributions of filler particles were investigated, and the evolution of the gaps between the particles was predicted by SPC, and compared with results from the detailed FEA. The related change in resistance was then modeled for both cases, using the random network model. The difference in behavior predicted by the two models was investigated by exploring a range of geometries, including variations of: (1) orientation or angles between nanoparticles and with respect to the tensile axis; and (2) initial gap size distribution. For the purposes of this discussion, the data from FEA is assumed to be correct and the simplified SPC model is compared with the FEA yardstick. The overall resistance of the material was tracked with increased strain, with particular focus on whether resistance was predicted to increase or decrease.

For the initial comparison of the models with differing nanoparticle orientations, the initial gap distribution was a random distribution with values evenly distributed between 3-7nm. The nanoparticles were assigned angles randomly distributed on a sphere for the orientation with

respect to the tensile axis (θ and ϕ), and also for the rotation of each nanoparticle (α and β). See Figure 2-3 for a detailed explanation of the angles. In this case, SPC predicted a change in resistance comparable in magnitude and slope to FEA. As seen in Figure 3-1, both gap orientation models predicted that resistance would decrease with strain, matching typical experimental results of the sensors. While there are discrepancies in the actual resistivity values, the trends are similar. This suggests that SPC may sufficient for modeling the conductive behavior of such materials, if only rough trends are required, when the particles are randomly oriented.

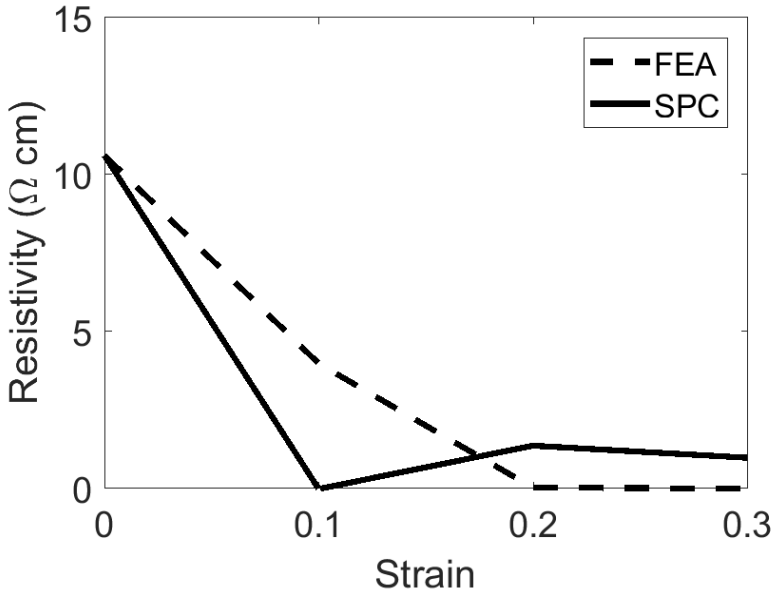

Figure 3-1. Resistivity versus strain for FEA and SPC. The angles for this test were randomly selected on a sphere and the same angles and initial gap sizes were used for both FEA and SPC.

The second example of potential nanoparticle geometry examined the case where particle orientations were restricted to a certain range. Using angles only within a certain range is representative of aligning the nanoparticles within the sensor during the manufacturing process.

The rotations of the nanoparticles (α and β in Figure 2-3), which are represented in FEA but not in SPC, appeared to have a significant impact on overall resistivity. One specific case where SPC differed from FEA occurred when all nanoparticles were perpendicular to the tensile direction, i.e. θ equal to 0° and ϕ equal to 90°±15° (see Figure 2-3). SPC predicted that all gaps would increase, causing the overall resistance to increase with strain. In FEA, most of the orientations had gap sizes that increased with strain, however, distributions of orientations where α and β were between 60-90° had gaps that decreased with strain causing the overall resistivity to decrease with strain (see Figure 3-2). Even small numbers of gaps that decrease in resistivity can have a big impact on overall resistivity.

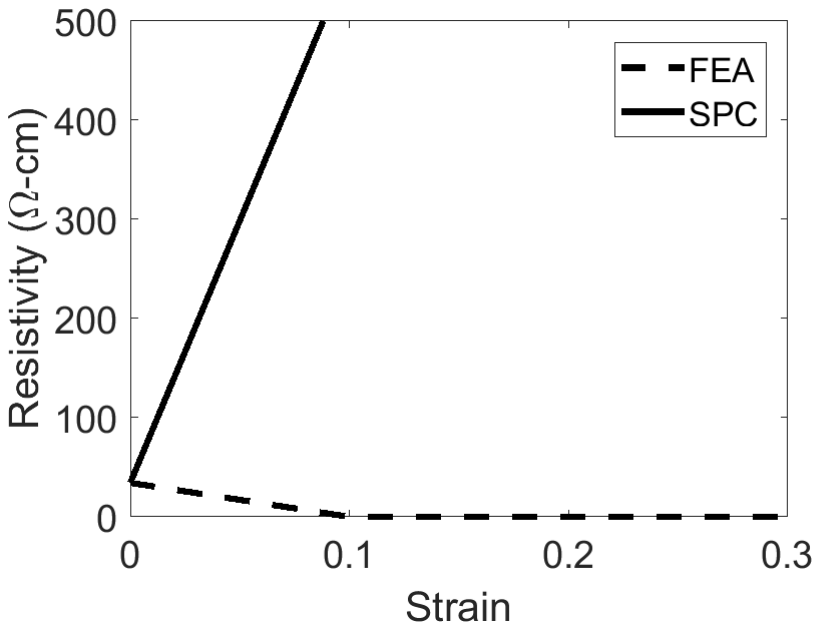

Figure 3-2. Resistance versus strain for FEA and SPC where angles are restricted to within 15° of the tensile axis and α and β in FEA are between 60-90°. SPC predicts a different trend between strain and resistance than FEA in this case but is similar in all other cases.

In order to understand more specifically which orientations of particles behaved differently in the FEA vs the SPC models, the azimuthal (θ) angle (see Figure 2-3) was varied for a particular strain (10% tensile strain), with all gaps set to the same initial value (5nm). Figure 3-3 and Figure 3-4 show how the distance between nanoparticles (or gap size) changes with strain, for different angles (i.e. particle alignments with the tensile axis). The angles θ and ϕ were combined into a single angle to match the variables defined in the SPC model [30]. The variance in the boxplot for the FEA data comes from the variations of the additional angles defined in the FEA data, i.e. the rotation of each of the nanoparticles or α and β; since the SPC model does not include these additional variables, there is no variance in the predicted result from this model. In each box of the boxplot, the middle line represents the median and the top and bottom lines represent the 75^{th} and 25^{th} percentiles, respectively. Outliers are shown by the red crosses. The difference between FEA and SPC is more pronounced at larger initial gap distances, leading to the selection of the relatively large initial gap size of 5nm for this comparison.

Because of the nature of the tunneling phenomenon (Equation 2), the smaller gaps correlate with large changes in resistance. When gaps are smaller than 2-3nm, the resistivity drops dramatically and the gap can conduct electricity. With the SPC model (Figure 3-4), there are no gaps that reach this range after 10% strain; the most significant decrease is a change in gap from 5nm to 4.75nm when the orientation is 90° from the tensile axis. On the other hand, the FEA data (Figure 3-3) predicts that some gaps at every orientation come close to the 2-3nm (highly conductive) range. Although it is mostly outliers in the boxplot that become conductive, even having a small number of conductive gaps has a large impact on overall resistivity.

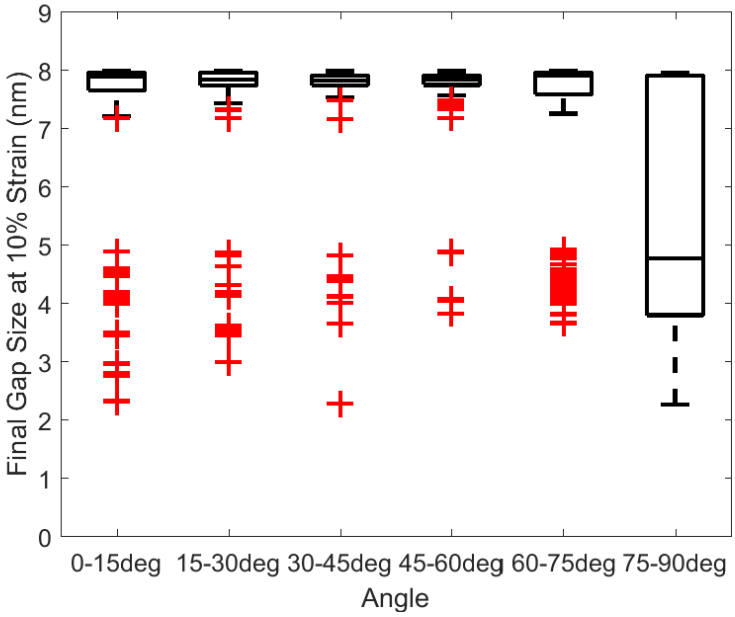

Figure 3-3. Boxplot showing final gap size (at 10% strain) versus angle between nanoparticles for data from FEA.

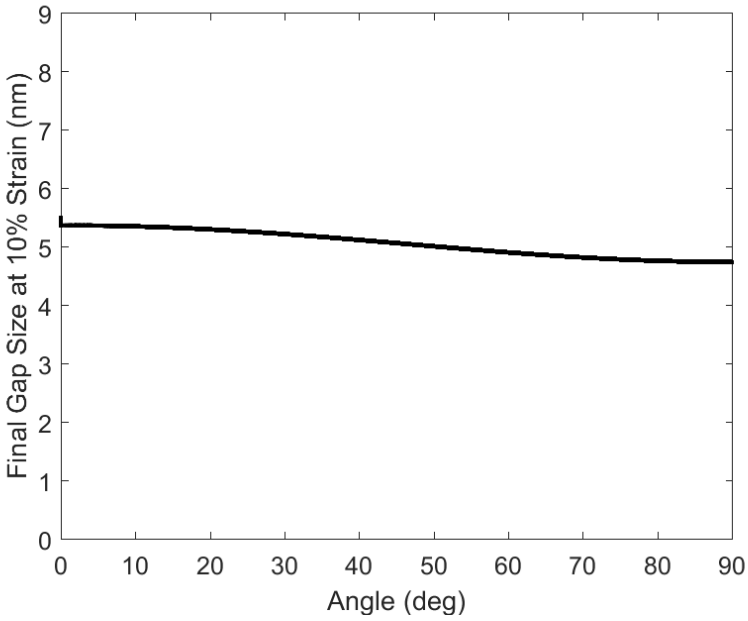

Figure 3-4. Change in gap size at 10% strain versus angle between nanoparticles for SPC.

Figure 3-3 and Figure 3-4 show that the rotations of nanoparticles (α and β) are important variables to include the full behavior of nanoparticles in order for a model to be accurate. When the particles are randomly oriented, the SPC representation may be incorrect for specific orientations, but the error averages out, resulting in approximately trends of resistivity vs strain (Figure 3-1); but for aligned particles the error is magnified (Figure 3-2).

3.1.2 Initial Gap Distribution

Another comparison between FEA and SPC tested the impact of different initial gap distributions on the overall resistivity evolution with strain. The different distributions tested were: uniform random, normal, delta, and Weibull. Johnson [31] used a Weibull distribution for his model using SPC, noting that others have used Weibull distributions to represent particle size distribution. Figure 3-5 shows the impact of size distribution on overall sensor resistivity. The angles of the nanoparticles in Figure 3-5 were again randomly distributed across a sphere. The impact was so significant that the data is best represented on a log scale for resistivity. All distributions used a mean of 5nm and a standard deviation (where applicable) of 0.67nm. The selected standard deviation ensured that almost all gaps (99.7%) were within 2nm of the mean.

The same initial gap distribution and sizes were used for both plots, so the initial resistivities start at the same values. While both the FEA and SPC show downward trends in resistivity, the resistivity decreases more sharply with strain with FEA. The sharper decrease in FEA makes sense because the FEA data predicts more gaps decreasing to a conductive range even at larger initial gap distances. When there are more individual resistivities in the random resistor network that are within a conductive range it will decrease the overall resistivity.

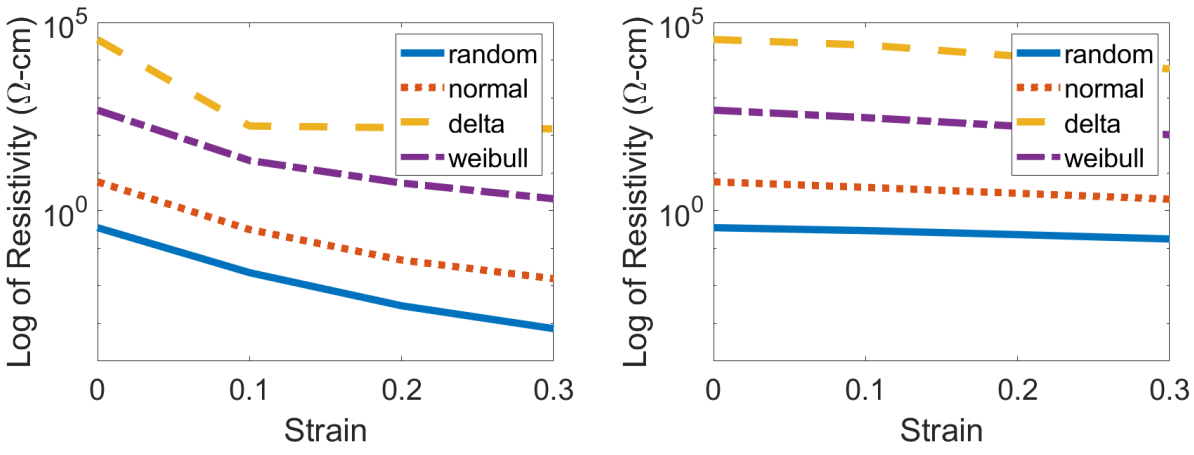

(a) (b)

Figure 3-5. Evidence of the impact of varying initial gap size distributions in (a) FEA data and (b) SPC. Note that both graphs are semi-logarithmic plots with the y-axis on a log scale.

Figure 3-6 shows another comparison using FEA data where the means of each of the distributions was altered so that the initial resistivity was the same. The mean of the delta distribution was kept the same as in Figure 3-5 (3.0nm) and the means of the other distributions were changed to match initial resistivity. The means used were: 4.5nm for the uniform random distribution, 4.0nm for the normal distribution, 3.0nm for the delta distribution, and 3.4nm for the Weibull distribution. All of the distributions follow the same trend (resistivity decreases with strain) but the shapes are different as well as the magnitude of the change in resistivity with strain. Figure 3-6 emphasizes the different responses to strain for the different distributions, even if each initial gap size distribution starts with the same initial resistivity. It seems clear that the initial gap size distribution used in the random resistor network has a significant impact on the resistivity versus strain behavior.

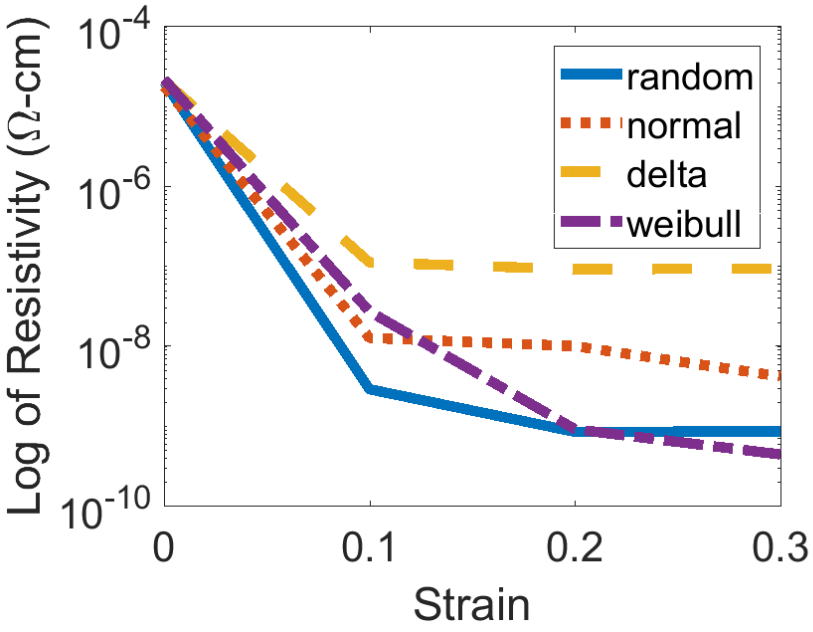

Figure 3-6. The means of the distributions were altered to start at the same initial resistivity. All distributions predict that resistivity decreases with strain, but there are major differences between different distributions. The means used were 4.5nm for uniform random, 4.0nm for normal, 3.0 nm for delta, and 3.4nm for Weibull.

The trends in the overall resistivities with strain for the different initial gap distributions correlates with what fraction of the initial gaps are small (i.e. around 2-3 nm). Figure 3-7 shows probability density functions for each of the distributions. The uniform random distribution has the highest number of initial gaps within the highly conductive 2-3nm range, so the overall resistivity is lower than any other distribution in Figure 3-5. Conversely, the delta function assigns none of the initial gaps to be in this 2-3nm range, and hence the overall resistivity is orders of magnitude higher than the other distributions.

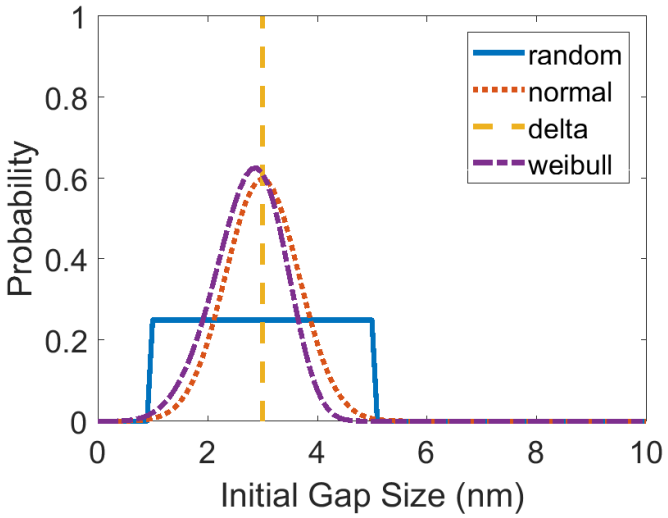

Figure 3-7. Probability density functions of the distributions used in Figure 3-5.

The value of the mean for a given distribution also has a large impact on resistivity. Figure 3-8 shows how resistivity changes for different values of initial mean gap. All initial gap size distributions in Figure 3-8 use normal distributions with a standard deviation of 0.67nm. Again, the graphs have log scales for resistivity.

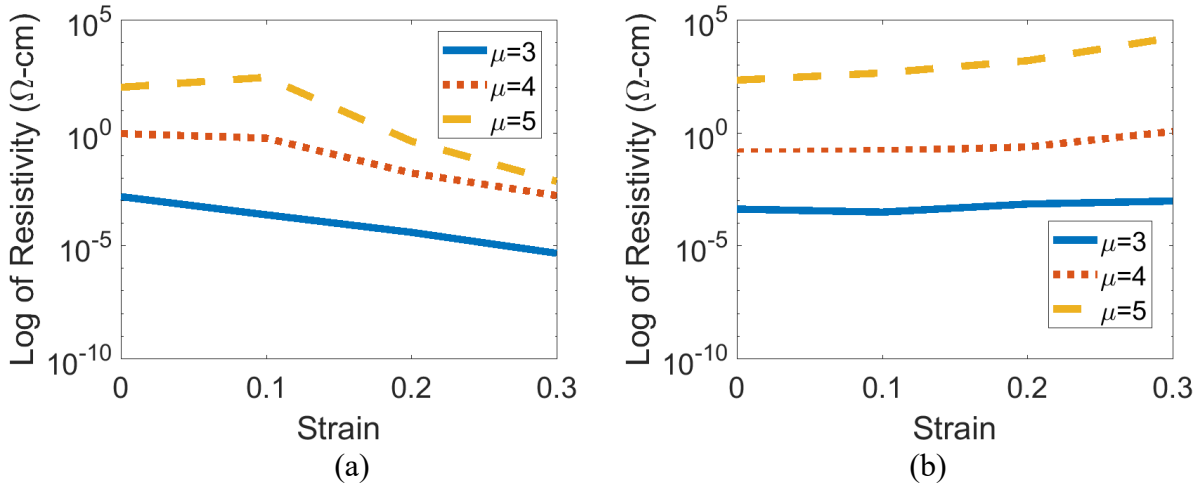

Figure 3-8. Impact of changing the mean in a normal distribution for (a) FEA and (b) SPC.

In summary, both the initial gap size distribution and the mean of that distribution significantly impact how the resistivity changes with strain. The differences between different mean gaps, and different types of distribution, can cause changes in resistivity of several orders of magnitude. The initial gap distributions that assign more gaps to the highly conductive range (smaller than about 2-3nm) have lower initial resistivities. Similarly, the smaller the value of the mean of the distribution, the more gaps are closer to the conductive range and the lower the initial resistivity. The sensitivity of resistivity to initial gap and particle orientation distribution suggests the potential to select variables for optimal response in a given sensor application.

3.2 Percolation Theory

The percolative behavior of this material with respect to volume fraction of filler has been well-established. As a critical volume fraction (the percolation threshold) of filler is reached, the conductivity increases rapidly as conductive pathways are formed across the sample. One could think about this in terms of an initial empty network spanning the polymer sample. As the volume fraction of filler increases, more connections in the network are 'switched on' by the presence of the filler. Eventually, enough connections are formed that a continuous pathway spans the sample, and conductivity starts to rise significantly.

Similarly, for the strained sample, the hypothetical empty network represents the gaps between the particles. As gaps close under Poisson contraction, the conductivity increases exponential, according to the quantum tunneling model. It has been hypothesized that this behavior results in a percolation type behavior – i.e. at a certain strain, the number of 'closed' gaps (gaps that are small enough to result in high conductivity – i.e. in the range of 2-3nm or less) reaches a critical fraction, and conductive paths form, rapidly increasing conductivity. If the

system follows percolation type behavior, there should be the typical s-curve for the conductance increase with strain.

Figure 3-9 and Figure 3-10 show how conductance is affected by gap size and strain. These plots should show the typical s-curve if percolation behavior plays a prominent role. Gaps were considered 'conductive' with a distance of 2nm or smaller for these figures. Both figures used the random resistor network with angles randomly distributed along a sphere and a uniform random distribution for the initial gap size with values between 2-7nm. The strain was between 0-0.3, which is a typical range of use for the conductive polymer sensors. As expected for a percolation-governed system, the conductance increases significantly once the fraction of gaps within the conductive range passes a certain critical value (see Figure 3-9). Although the fraction of conductive gaps does not increase beyond 10 percent, the conductivity rises from almost zero to nearly 15 Siemens. It is also important to note that there is a clear s-curve in Figure 3-9 which leads to percolation being an important part to describe this phenomenon.

Figure 3-10 shows conductance versus strain for two different random variations of the same model. The plot on the left shows a slight s-curve starting at almost zero strain which suggests that the behavior follows percolation theory. However, the plot on the right does not show a clear s-curve. Figure 3-10 shows two examples of random orientations in the random resistor network model. While neither curve is a strong s-curve, it still does not rule out percolation theory as a necessary piece to describe the behavior of nanocomposite sensors.

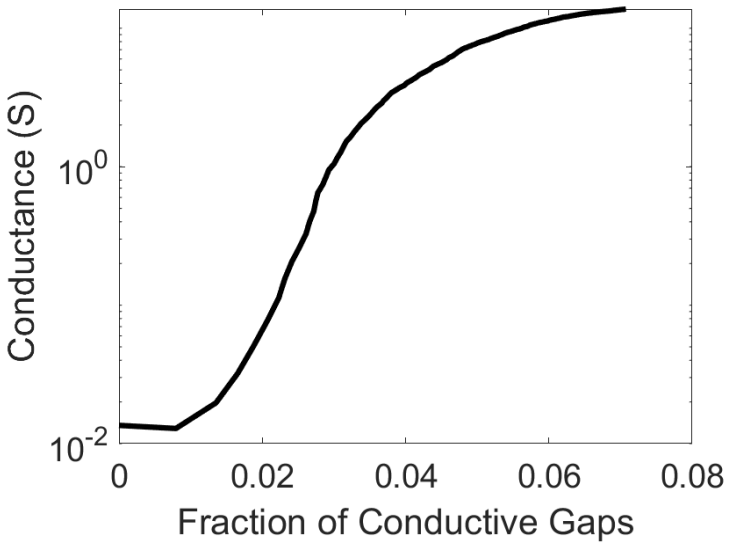

Figure 3-9. Conductance versus the fraction of gaps with a distance less than 2nm. The conductance increases as more gaps become conductive, as expected.

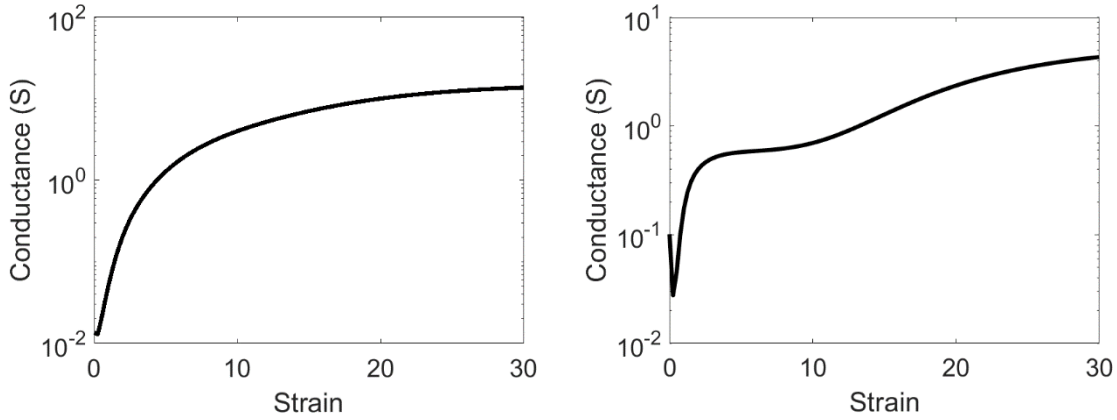

Figure 3-10. Conductance versus strain on a log plot. If this resistor network system follows percolative behavior, these graphs should show an s-curve. The plot on the left shows slight s-curve behavior around 0 strain, but not enough to conclude that percolation theory is necessary.

In order to further evaluate the relevance of percolation theory in the electrical behavior of the sensors, the resistivity-strain behavior of the random resistor network was compared to the generalized effective medium (GEM) equation (see Equation 2) and the effective medium (EM) equation. The EM equation removes the percolation theory parts of the GEM, as shown in

Equation 5, where ϕ is the volume fraction of filler, σ_m is the conductivity of the neat polymer matrix, σ_f is the conductivity of the filler material, σ_b is the conductivity of the bulk material, and n is the dimensionality (3D for the sensor material).

$$(1-\phi)\frac{(\sigma_m-\sigma_b)}{\sigma_m+(n-1)\sigma_b}+\phi\frac{(\sigma_f-\sigma_b)}{\sigma_f+(n-1)\sigma_b}=0 \quad 5$$

Figure 3-11 shows the random resistor network (RRN) compared to the GEM and EM. The random resistor network in this figure used a delta function for the initial gap distribution with a value of 3nm. The values for variables in the GEM/EM equations were taken from Johnson [21] or fit with a least squares approach and are shown in Table 3-1. Figure 3-11 shows that the GEM equation fits much more closely to the RRN than the EM equation. This suggests that the piezoresistive effects in the RRN that are not fully captured by simply using the EM equation and confirms that the conductance-strain relationship does follow percolation type behavior.

Table 3-1. Values for the generalized effective medium (GEM) and effective medium (EM) equations used in Figure 3-11. See Equation 2 for GEM and Equation 5 for EM.

Variable	*Value*	*Source*
$\boldsymbol{\sigma_m}$	1.11e-8	Least Squares Fit
$\boldsymbol{\sigma_f}$	2.72e2	[21]
$\boldsymbol{s}$	10.37	[21]
$\boldsymbol{t}$	1.72	[21]
$\boldsymbol{\phi_c}$	0.0045	[21]

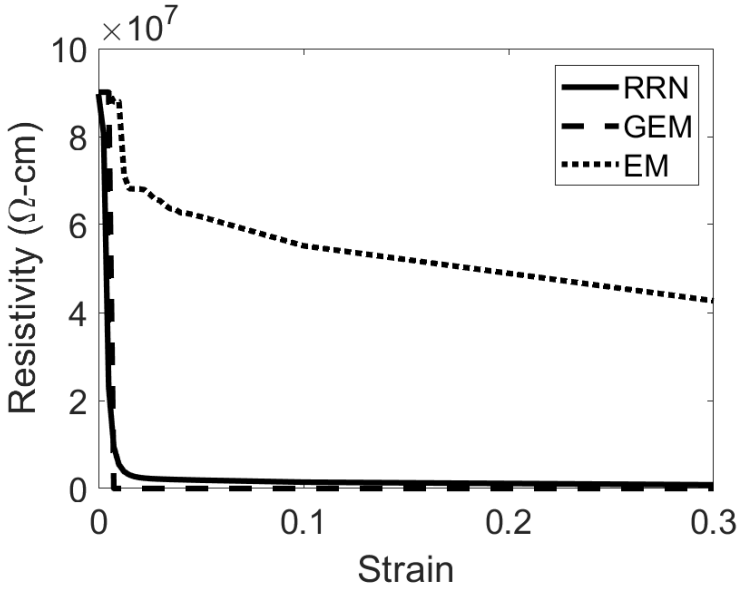

Figure 3-11. Resistivity-strain curves for the random resistor network (RRN) compared to the generalized effective medium (GEM) equation with percolation and the effective medium (EM) equation without percolation theory.

3.3 Experimental Verification

The random resistor network (RRN) was validated by comparing the model to resistivity data of an actual nanocomposite sensor. The sensor tested was made of Sylgard 184 with 15% nickel nanoparticles by volume and the resistivity was measured for values of strain between 0 and 60 percent. The dots in Figure 3-12 show the experimental data and the lines show the RRN model using FEA and SPC. The overall shape of the RRN model changes significantly ased on the parameters input to the model and the random arrangement of resistances within the network. Even when running the same parameters for nanoparticle angles and initial gap size distribution, the overall shape of the resistivity-strain curve will vary because different resistors end up in different locations. The curve in Figure 3-12 also used a cut-off for the minimum gap distance as 1nm rather than 2nm for the RRN model as well as using a linear extrapolation for the FEA data

rather than the exponential fit described previously. The FEA curve in Figure 3-12 represents a best fit with the smallest square error for the RRN model with FEA when compared with the experimental data. The RRN model with SPC is shown as a comparison using the same parameters including the number of resistors, angles assigned, and initial gap size distribution.

Figure 3-12 used angles for nanoparticle orientation that were randomly distributed along a sphere in the RRN. In Figure 3-12, the distribution for initial gap sizes was a Weibull distribution with a scaling parameter of 3.5nm and a shape parameter of 12.36 (the same value used in Johnson [30]). The mean for the Weibull distribution seems reasonable because it puts initial gap sizes between 1.5nm and 4.2nm. Having one molecule of polymer between two nanoparticles would be 1nm, but there are most likely some gaps that have more than just one molecule between the two nanoparticles. The range of gap sizes with this Weibull distribution seems representative of what could actually happen with polymer gaps between nanoparticles.

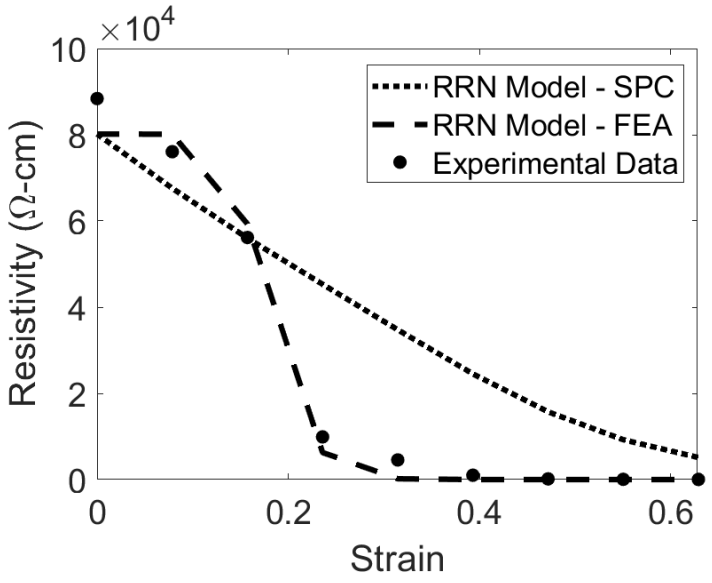

Figure 3-12. Resistivity-strain comparison between experimental data and the random resistor network (RRN) for the best fit. The RRN used angles for nanoparticle orientation randomly distributed along a sphere and a Weibull distribution with a mean of 3.5nm for the initial gap size distribution and a shape parameter of 12.36 (see [30]).

Figure 3-12 compares the performance of the FEA-based gap evolution model with the SPC model for a real sensor. For both models, the alignment and gap distribution was allowed to vary in order to line up with the real data. But only the FEA model was able to find a nanoparticle arrangement that resulted in a close match between predicted and actual resistivity. As noted previously (see Figure 3-3 and Figure 3-4), the FEA model predicts larger decreases in gap size for a few junctions, even when the relatively large starting gap of 5nm is chosen; the SPC model predicts a much more homogeneous change in gap size.

3.4 Design Problem – Gauge Factor

As shown earlier, the orientation of nanoparticles can have a significant impact on resistivity change with strain. From a design perspective, it would be helpful to know, then, what the best orientation of nanoparticles would be to get the greatest gauge factor, or change in resistivity for a certain change in strain. The orientations tested were (1) random selection of rotations (defined by θ and ϕ) on the sphere, (2) selecting initial nanoparticle axes (y'' in Figure 2-3) within ±15° of parallel to the tensile axis, (3) selecting initial nanoparticle axes within ±45° from the tensile axis, and (4) selecting initial nanoparticle axes within ±15° of perpendicular to the tensile axis. Within these orientation definitions, varying angles for the rotations of individual nanoparticles (defined by α and β) were also assumed, viz. random rotations, rotations between 0-30°, or rotations between 60-90°.

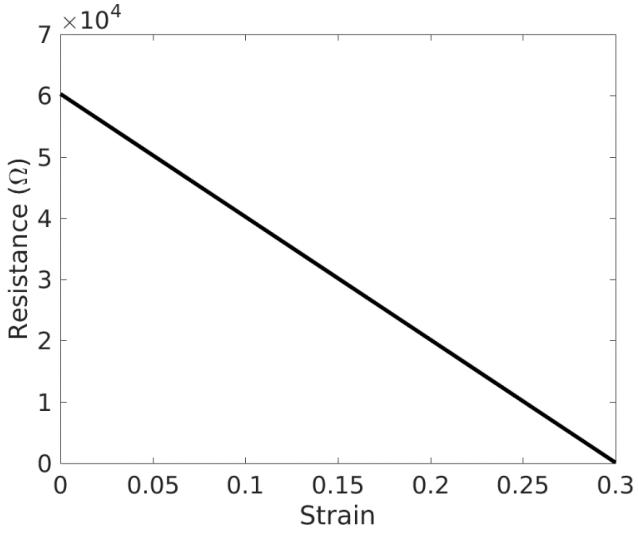

Figure 3-13. Resistivity vs strain for random rotations described by θ and ϕ, but α and β lie between 0-30^o (the particles are aligned relative to each other).

The highest gauge factor, and largest change in resistivity, came from using all possible orientations for the nanoparticle axes (θ and ϕ randomly distributed along a sphere) but restricting the rotations of the nanoparticles to between 0-30° (i.e. by aligning the nanoparticles relative to each other, but not relative to the global frame). Allowing α and β to be any possible values (rather than the range between 0-30°) decreased the gauge factor by 0.5-1. The gauge factor for the example in Figure 3-13 is 3.

3.5 Design Problem – Initial Rise in Resistivity

One phenomenon that happens in the silicone-nickel nanoparticle sensors studied in related work [54] is an initial rise in resistance at small values of strain. Figure 3-14 shows a curve with the characteristic initial rise in resistivity using the RRN model with FEA. The curve in Figure 3-14 used angles for nanoparticle orientation randomly distributed along a sphere and a Weibull distribution for initial gap sizes with a scaling parameter of 7nm and a shaping parameter of

12.36. The initial spike in resistivity happened with other ranges for the orientation of nanoparticles such as nanoparticles axes within ±45° or ±15°of the tensile axis. The spike happened regardless of the initial gap distribution or mean used, although using a large value for the mean value of initial gap caused the initial resistance rise to be more pronounced. It is also important to note that not every resistivity-strain curve from the RRN model shows the initial rise in resistivity. Most of the figures used in this work were chosen because they did not show the initial spike in resistivity, although seeing the spike in resistivity was more frequent in results than not.

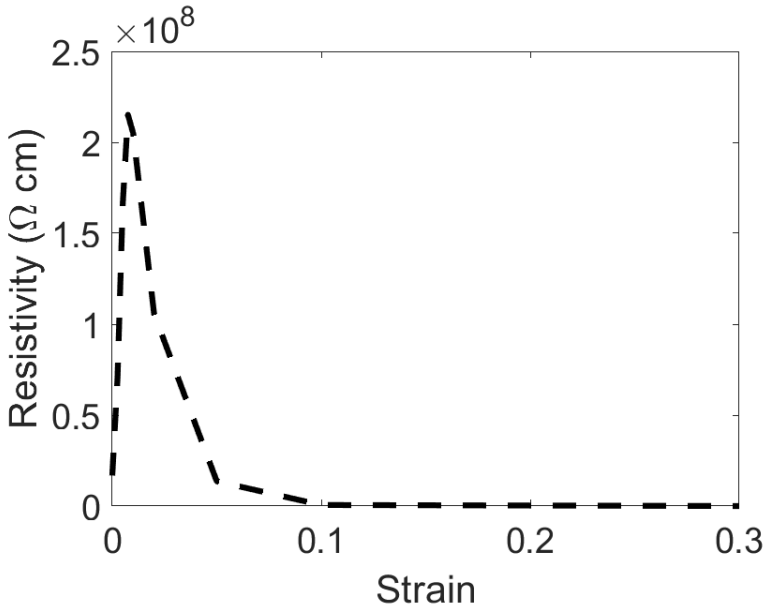

Figure 3-14. A resistivity-strain curve that shows the characteristic initial increase in resistivity seen in experimental data from sensors. This curve used a Weibull distribution with a scaling parameter of 7nm and a shaping parameter of 12.36.

While it is a good sign that the RRN model with FEA can replicate the initial increase in resistivity, it would be better to find a way to get rid of this effect. Different ranges of angles between nanoparticles were tested to attempt to find a particular range that would eliminate the

initial rise in resistance. When α and β were restricted to be within 0-30°, θ restricted within ±15° of the tensile axis, and ϕ within ±15° of 90° (see Figure 2-3), the initial spike in resistivity disappeared. Figure 3-15 shows an example of one curve with the described restriction in angles.

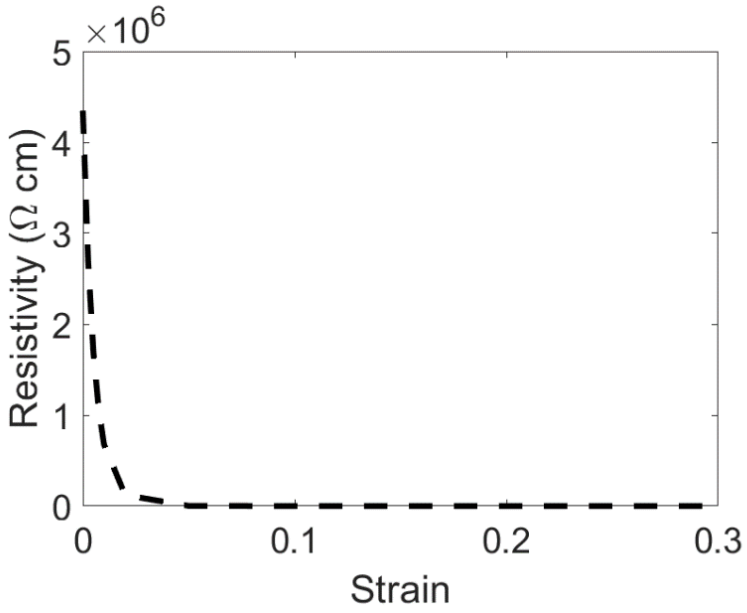

Figure 3-15. Resistivity-strain curve where angles between nanoparticles are restricted to 0-30° for α and β, ±15° of parallel to the tensile axis for θ, and between 75-90° for ϕ. The initial spike in resistance was eliminated when the angles were restricted to the ranges described.

The fact that these angle restrictions eliminated the initial increase in resistivity makes sense since all gaps between nanoparticles at these orientations should decrease with strain according to Poisson's contraction (see Figure 2-3). Hence, it seems that if there were a way to restrict the angles between nanoparticles to a particular range of desired values that it would be possible to remove the unwanted initial spike in resistivity at small values of strain.

4 SUMMARY AND CONCLUSION

The electrical behavior under strain for a nanocomposite sensor was modeled using a random resistor network where the resistance of each polymer gap between two nanoparticles was found using quantum tunneling. The two questions that this model sought to answer were: (1) Does a simple Poisson contraction model of the evolution of the gap between nanoparticles adequately capture the physical behavior in order to accurately predict the resistance-strain relationship of the overall sensor, or is a more complex model required? and (2) Is the piezoresistivity in the sensor best modeled with percolation theory or is a standard effective medium type approach sufficient?

In order to analyze the evolution of the gap between nanoparticles, two models were compared: Finite Element Analysis (FEA) and Simple Poisson's Contraction (SPC). The FEA data modeled each nanoparticle as a cylinder in a silicone matrix. While the cylindrical assumption may not be totally physically accurate, the high aspect ratio of the particles means that any effects from particle curvature are at a distance. There may also be effects from the branched nature of the nanoparticles, but these branching effects would show up in terms of relative alignment of the neighboring nanoparticles. SPC assumed that the nanoparticles and matrix could be modeled as a homogenous material and applied Poisson's contraction to predict gap change with global strain. Despite the simpler approach, SPC proved to be effective at capturing the general strain-resistivity behavior for a typical case where particles were randomly

oriented. In more specialized cases (e.g. aligning nanoparticles), SPC diverges significant from actual behavior modeled using FEA; for example, SPC predicts that the overall resistivity would increase in various scenarios where FEA shows that it actually decreases. The difference between SPC and FEA stems from the fact that SPC only considers the orientation of the shortest vector between the particles (given by θ and ϕ), without considering the relative orientations of the particles (with respect to the tensile direction, for example). FEA demonstrates that a subset of gaps decreases with strain for a range of θ and ϕ orientations, when the SPC would only predict gap increase for many of these cases. Overall FEA predicts that gaps become 'conductive' (i.e. decrease to around 2nm) from larger initial gap sizes and for a broader number of orientations, compared with SPC.

FEA provided interesting insight into the behavior of nanoparticles at specific orientations with respect to each other and the tensile axis. FEA showed that at large values of initial gap distance for certain orientations of nanoparticles, the polymer gap will decrease enough for the gap to be conductive (less than about 2nm). The evolution of gap distances with strain from SPC showed a much more subtle change in gap with strain. The mean value of the initial gap distribution impacts the initial value of the overall resistivity. A lower value for the mean assigns more initial gaps closer to the conductive region which decreases the overall resistivity. The nature of the initial distribution influences the shape of the resistivity-strain curve, as well as the initial value for resistivity. The order from least to greatest initial resistivity for different distributions was uniform random, normal, Weibull, delta. The differences in initial resistivity between different distributions directly relates to the number of gaps that start in the conductive region. Because the overall resistivity is so sensitive to the initial gap distribution, the ability to empirically determine the general distribution of initial gap sizes would greatly

enhance the accuracy of the model. There are obviously difficulties with this idea, such as the nano-size scale. Given that it would be a huge effort to extract nano-scale measurement of gap across a large number of junctions (if it were even possible), the more accurate FEA / RRN model may allow the distribution to be inferred by comparing actual behavior to modeled behavior.

The detailed understanding of how orientation affects gap size available with FEA makes it possible to design a sensor with desired characteristics. The highest gauge factor can be achieved by using all possible orientations for nanoparticles, i.e. angles randomly distributed along a sphere. The initial increase in resistivity seen in real sensors seen in real sensors can be removed by assuming particle geometry where α and β were restricted to be within 0-30°, θ restricted within ±15° of the tensile axis, and ϕ within ±15° of 90°. This range of orientation for the nanoparticles should have all gaps decrease according to Poisson's contraction, so it follows that the overall resistivity would decrease.

Another question answered by this study related to whether the material response of the sensor followed percolation theory. The conductance-strain relationship showed a characteristic s-curve expected in percolative system. There was also an s-curve when plotting conductance versus the fraction of conductive gaps. Finally, the generalized effective medium equation (GEM) was found to fit the random resistor network much more closely than the effective medium equation. From these findings, it can be concluded that the system does follow a percolation response, and, therefore, modeling the piezoresistivity with percolation theory accurately models the material response.

REFERENCES

1. Duan, H., et al., *Ultrahigh molecular weight polyethylene composites with segregated nickel conductive network for highly efficient electromagnetic interference shielding.* Materials Letters, 2017. **209**: p. 353-356.

2. Zhao, B., et al., *Flexible, Ultrathin, and High-Efficiency Electromagnetic Shielding Properties of Poly (vinylidene fluoride)/Carbon Composite Films.* ACS Applied Materials & Interfaces, 2017.

3. Barton, R., J. Keith, and J. King, *Development and modeling of electrically conductive carbon filled liquid crystal polymer composites for fuel cell bipolar plate applications.* Journal of New Materials for Electrochemical Systems, 2007. **10**(4): p. 225.

4. Wang, M.-H., et al., *Direct electrodeposition of Graphene enhanced conductive polymer on microelectrode for biosensing application.* Biosensors and Bioelectronics, 2018. **99**: p. 99-107.

5. Shiri, H.M., A. Ehsani, and M.J. Khales, *Electrochemical synthesis of Sm2O3 nanoparticles: Application in conductive polymer composite films for supercapacitors.* Journal of Colloid and Interface Science, 2017. **505**: p. 940-946.

6. Hui, C., et al., *Characteristics and preparation of polymer/graphite composite bipolar plate for PEM fuel cells.* Journal of composite materials, 2009. **43**(7): p. 755-767.

7. Keith, J., J. King, and B. Johnson, *Electrical conductivity modeling of carbon filled polypropylene based resins for fuel cell bipolar plate applications.* Journal of New Materials for Electrochemical Systems, 2008. **11**(4): p. 253-257.

8. Johnson, T.M., D.T. Fullwood, and G. Hansen, *Strain monitoring of carbon fiber composite via embedded nickel nano-particles.* Composites Part B: Engineering, 2012. **43**(3): p. 1155-1163.

9. Amjadi, M., et al., *Stretchable, Skin-Mountable, and Wearable Strain Sensors and Their Potential Applications: A Review.* Advanced Functional Materials, 2016.

10. Lei, H., et al., *Modeling carbon black/polymer composite sensors.* Sensors and Actuators B: Chemical, 2007. **125**(2): p. 396-407.

11. Amjadi, M., Y.J. Yoon, and I. Park, *Ultra-stretchable and skin-mountable strain sensors using carbon nanotubes–Ecoflex nanocomposites.* Nanotechnology, 2015. **26**(37): p. 375501.

12. Gong, S., et al., *Highly Stretchy Black Gold E-Skin Nanopatches as Highly Sensitive Wearable Biomedical Sensors.* Advanced Electronic Materials, 2015. **1**(4).

13. Boland, C.S., et al., *Sensitive, high-strain, high-rate bodily motion sensors based on graphene–rubber composites.* ACS nano, 2014. **8**(9): p. 8819-8830.

14. Kong, J.-H., et al., *Simple and rapid micropatterning of conductive carbon composites and its application to elastic strain sensors.* Carbon, 2014. **77**: p. 199-207.

15. Lu, N., et al., *Highly sensitive skin-mountable strain gauges based entirely on elastomers.* Advanced Functional Materials, 2012. **22**(19): p. 4044-4050.

16. Bergström, J. and M. Boyce, *Constitutive modeling of the large strain time-dependent behavior of elastomers.* Journal of the Mechanics and Physics of Solids, 1998. **46**(5): p. 931-954.

17. Park, J., et al., *Giant tunneling piezoresistance of composite elastomers with interlocked microdome arrays for ultrasensitive and multimodal electronic skins.* ACS nano, 2014. **8**(5): p. 4689-4697.

18. Shin, U.-H., et al., *Highly stretchable conductors and piezocapacitive strain gauges based on simple contact-transfer patterning of carbon nanotube forests.* Carbon, 2014. **80**: p. 396-404.

19. Dang, Z.-M., et al., *Supersensitive linear piezoresistive property in carbon nanotubes/ silicone rubber nanocomposites.* Journal of Applied physics, 2008. **104**(2): p. 024114.

20. Yao, S. and Y. Zhu, *Wearable multifunctional sensors using printed stretchable conductors made of silver nanowires.* Nanoscale, 2014. **6**(4): p. 2345-2352.

21. Hicks, J., A. Behnam, and A. Ural, *Resistivity in percolation networks of one-dimensional elements with a length distribution.* Physical Review E, 2009. **79**(1): p. 012102.

22. Hecht, D., L. Hu, and G. Grüner, *Conductivity scaling with bundle length and diameter in single walled carbon nanotube networks.* Applied Physics Letters, 2006. **89**(13): p. 133112.

23. Ma, H. and X.-L. Gao, *A three-dimensional Monte Carlo model for electrically conductive polymer matrix composites filled with curved fibers.* Polymer, 2008. **49**(19): p. 4230-4238.

24. Zhang, J., et al., *Electrical and dielectric behaviors and their origins in the three-dimensional polyvinyl alcohol/MWCNT composites with low percolation threshold.* Carbon, 2009. **47**(5): p. 1311-1320.

25. Zeng, Q., A. Yu, and G. Lu, *Multiscale modeling and simulation of polymer nanocomposites.* Progress in polymer science, 2008. **33**(2): p. 191-269.

26. Ambrosetti, G., et al., *Solution of the tunneling-percolation problem in the nanocomposite regime.* Physical Review B, 2010. **81**(15): p. 155434.

27. Oskouyi, A., U. Sundararaj, and P. Mertiny, *Tunneling conductivity and piezoresistivity of composites containing randomly dispersed conductive nano-platelets.* Materials, 2014. **7**(4): p. 2501-2521.

28. Raina, A. and C. Linder, *A homogenization approach for nonwoven materials based on fiber undulations and reorientation.* Journal of the Mechanics and Physics of Solids, 2014. **65**: p. 12-34.

29. Chung, D., *Carbon materials for structural self-sensing, electromagnetic shielding and thermal interfacing.* Carbon, 2012. **50**(9): p. 3342-3353.

30. Johnson, O.K., et al., *Multiscale model for the extreme piezoresistivity in silicone/nickel nanostrand nanocomposites.* Metallurgical and Materials Transactions A, 2011. **42**(13): p. 3898-3906.

31. Kalantari, M., et al., *A new approach for modeling piezoresistive force sensors based on semiconductive polymer composites.* IEEE/ASME Transactions on Mechatronics, 2012. **17**(3): p. 572-581.

32. Luheng, W., D. Tianhuai, and W. Peng, *Influence of carbon black concentration on piezoresistivity for carbon-black-filled silicone rubber composite.* Carbon, 2009. **47**(14): p. 3151-3157.

33. Paredes-Madrid, L., et al., *Underlying Physics of Conductive Polymer Composites and Force Sensing Resistors (FSRs) under Static Loading Conditions.* Sensors, 2017. **17**(9): p. 2108.

34. Zhang, X.W., et al., *Time dependence of piezoresistance for the conductor-filled polymer composites.* Journal of Polymer Science part B: polymer physics, 2000. **38**(21): p. 2739-2749.

35. Hu, N., et al., *Tunneling effect in a polymer/carbon nanotube nanocomposite strain sensor.* Acta Materialia, 2008. **56**(13): p. 2929-2936.

36. Oskouyi, A.B., U. Sundararaj, and P. Mertiny, *Tunneling conductivity and piezoresistivity of composites containing randomly dispersed conductive nano-platelets.* Materials, 2014. **7**(4): p. 2501-2521.

37. Simmons, J.G., *Generalized formula for the electric tunnel effect between similar electrodes separated by a thin insulating film.* Journal of applied physics, 1963. **34**(6): p. 1793-1803.

38. Koecher, M., et al., *Characterization of nickel nanostrand nanocomposites through dielectric spectroscopy and nanoindentation.* Polymer Engineering & Science, 2013. **53**(12): p. 2666-2673.

39. *Conductive Composites*. [cited 2019 2/12/19]; Available from: http://www.conductivecomposites.com/.

40. Hansen, N., D.O. Adams, and D.T. Fullwood, *Quantitative methods for correlating dispersion and electrical conductivity in conductor–polymer nanostrand composites.* Composites Part A: Applied Science and Manufacturing, 2012. **43**(11): p. 1939-1946.

41. McLachlan, D., et al., *The correct modelling of the second order terms of the complex AC conductivity results for continuum percolation media, using a single phenomenological equation.* Physica B: Condensed Matter, 2003. **338**(1): p. 256-260.

42. Alig, I., et al., *Dynamic percolation of carbon nanotube agglomerates in a polymer matrix: comparison of different model approaches.* physica status solidi (b), 2008. **245**(10): p. 2264-2267.

43. Lysenkov, E. and V. Klepko, *Analysis of Percolation Behavior of Electrical Conductivity of the Systems Based on Polyethers and Carbon Nanotubes.* Journal of Nano-and Electronic Physics, 2016. **8**(1): p. 1017-1.

44. Yi, X.S., G. Wu, and Y. Pan, *Properties and applications of filled conductive polymer composites.* Polymer international, 1997. **44**(2): p. 117-124.

45. Deng, H., et al., *Effect of melting and crystallization on the conductive network in conductive polymer composites.* Polymer, 2009. **50**(15): p. 3747-3754.

46. Hussain, M., Y.-H. Choa, and K. Niihara, *Fabrication process and electrical behavior of novel pressure-sensitive composites.* Composites Part A: applied science and manufacturing, 2001. **32**(12): p. 1689-1696.

47. Zhou, J., et al., *Percolation transition and hydrostatic piezoresistance for carbon black filled poly (methylvinylsilioxane) vulcanizates.* Carbon, 2008. **46**(4): p. 679-691.

48. Xu, S., et al., *The viability and limitations of percolation theory in modeling the electrical behavior of carbon nanotube–polymer composites.* Nanotechnology, 2013. **24**(15): p. 155706.

49. Balberg, I., *Tunneling and nonuniversal conductivity in composite materials.* Physical Review Letters, 1987. **59**(12): p. 1305.

50. Rakowski, W.A. and M. Kot, *Thermal stress model for polymer sensors.* Journal of Thermal Stresses, 2004. **28**(1): p. 17-28.

51. Taya, M., W. Kim, and K. Ono, *Piezoresistivity of a short fiber/elastomer matrix composite.* Mechanics of materials, 1998. **28**(1): p. 53-59.

52. Johnson, O.K., et al., *Deciphering the structure of nano-nickel composites*. 2009, Los Alamos National Laboratory (LANL): SAMPE 2009.

53. Litvinov, V. and P. Steeman, *EPDM− Carbon Black interactions and the reinforcement mechanisms, as studied by low-resolution 1H NMR.* Macromolecules, 1999. **32**(25): p. 8476-8490.

54. Baradoy, D.A., *Composition Based Modaling of Silicone Nano-Composite Strain Gauges.* 2015.